Faraday Discussions

Cite this: *Faraday Discuss.*, 2021, **230**, 52

PAPER

Identification of C_2–C_5 products from CO_2 hydrogenation over $PdZn/TiO_2$–ZSM-5 hybrid catalysts†

Jonathan Ruiz Esquius, [a] Hasliza Bahruji, [b] Michael Bowker *[ac] and Graham J. Hutchings *[a]

Received 13th December 2020, Accepted 10th February 2021
DOI: 10.1039/d0fd00135j

The combination of a methanol synthesis catalyst and a solid acid catalyst opens the possibility to obtain olefins or paraffins directly from CO_2 and H_2 in one step. In this work several $PdZn/TiO_2$–ZSM-5 hybrid catalysts were employed under CO_2 hydrogenation conditions (240–360 °C, 20 bar, $CO_2/N_2/H_2 = 1:1:3$) for the synthesis of CH_3OH, consecutive dehydration to dimethyl ether and further oxygenate conversion to hydrocarbons. No significant changes after 36 h reaction on the methanol synthesis catalyst ($PdZn/TiO_2$) were observed by XRD, XAS or XPS. No olefins were observed, indicating that light olefins undergo further hydrogenation under the reaction conditions, yielding the corresponding alkanes. Increasing the aluminium sites in the zeolites (Si : Al ratio 80 : 1, 50 : 1 and 23 : 1) led to a higher concentration of mild Brønsted acid sites, promoting hydrocarbon chain growth.

Introduction

The sustainable production of energy is one of the major challenges of modern society.[1,2] Several technologies have been developed to harvest renewable energy (*e.g.*, solar panels, wind farms) in the form of electricity.[2] However, due to the intermittent nature of renewables, surplus produced electricity must be stored as chemical bonds to ensure a steady production of energy when electricity

[a]*School of Chemistry, Cardiff Catalysis Institute, Cardiff University, Main Building, Park Place, Cardiff CF10 3AT, UK. E-mail: Hutch@cardiff.ac.uk; BowkerM@cardiff.ac.uk*

[b]*Centre of Advanced Material and Energy Science, University Brunei Darussalam, Jalan Tungku Link, Gadong BE 1410, Brunei Darussalam*

[c]*Catalysis Hub, RCAH, Rutherford Appleton Laboratory, Harwell Oxford, Didcot OX11 0QX, UK*

† Electronic supplementary information (ESI) available: XRD, pore size and surface area for commercial ZSM-5 after activation (550 °C, 6 h). CO_2 reaction metrics. CO_2 hydrogenation activity over $PdZn/TiO_2$ at different temperatures, CO_2 hydrogenation over ZSM-5 (23 : 1). Productivities and hydrocarbon selectivity based on MTH/DMTH over $PdZn/TiO_2$–ZSM-5 hybrid catalysts. EXAFS fitting parameters. XRD and XPS post reaction $PdZn/TiO_2$ characterisation. Coke determination by TG-MS. See DOI: 10.1039/d0fd00135j

production is low.[3] The production of H_2 *via* water splitting is a route with a high renewable electricity storage capacity,[4] and is a possible energy vector for future technology.[5,6] However, energy decarbonisation is likely to occur in a subtle way.[7] Therefore, it is important to develop transitory routes that allow the use of current technology, but approach CO_2 neutrality.[8] This can be achieved by storing H_2 produced *via* water electrolysis through renewable electricity in the form of hydrocarbons, by its reaction with CO_2.[9–11]

The production of CH_3OH from syngas ($CO/CO_2/H_2$) over a $CuO/ZnO/Al_2O_3$ catalyst is a mature process (250–300 °C, 50–100 bar), with an annual CH_3OH production of 57 Mt,[10] and increasing. Hence, renewable H_2 could be easily incorporated in the CH_3OH production cycle, however for the process to be CO_2 neutral, CH_3OH must be obtained from recycled CO_2 and sustainably produced H_2. Thermodynamically, CH_3OH formation from CO_2 and H_2 is favoured at high pressure and low temperature. Nevertheless, a high temperature (>200 °C) is needed to activate CO_2, which in turn results in the deactivation of Cu-based catalysts due to Cu sintering[9–13] and coke deposition.[14] Pd-based catalysts are employed in CO_2 hydrogenation to CH_3OH as a stable alternative to Cu-based catalysts.[15–19]

Research on Pd/ZnO catalysts confirmed the β-PdZn alloy as the active phase for CH_3OH synthesis.[20–23] Commercially sourced ZnO usually has a low surface area which results in large PdZn particles, and hence, to improve PdZn dispersion, supports with a higher surface area (*e.g.*, CeO_2,[18] carbon nanofibers,[22] carbon nanotubes,[24] Al_2O_3,[25] or TiO_2 (ref. 25 and 26)) are commonly used. The higher stability of PdZn alloy catalysts allows for higher reaction temperatures, however, then CH_3OH productivity is limited by the thermodynamic equilibrium whilst CO formation is favoured through the reverse water gas shift (RWGS) reaction. To increase oxygenate productivity above the limited CO_2 hydrogenation to CH_3OH dictated by the equilibrium, CH_3OH can be simultaneously dehydrated to dimethyl ether (DME) by physically mixing a methanol synthesis catalyst with a solid acid catalyst.[27–30] ZSM-5 zeolites are commonly employed as solid acid catalysts to dehydrate CH_3OH to DME due to their high resistance to water, high stability and the presence of Lewis and Brønsted acid sites.[31] The conversion of methanol or dimethyl ether to hydrocarbons (MTH or DMTH respectively) is a mature process that also employs ZSM-5 zeolites as catalysts (300–500 °C, 1 bar).[32–34] More importantly, it has been reported that using H_2 or H_2O in the feed for the MTH process decreased the deactivation of several zeolites (HSAPO, HSSZ, HFER, HBEA, ZSM-5) by limiting coke deposition within structural pores, without significantly affecting the hydrocarbon chain distribution or the olefin-to-paraffin selectivity.[35–37] Water is produced as a by-product in CO_2 hydrogenation to CH_3OH, moreover H_2 is present in the feed. Hence, the synthesis of hydrocarbons from CO_2 over a methanol synthesis catalyst combined with an acid catalyst with reduced coke deposition is achievable. Bonura *et al.*[29] studied different reactor bed configurations for the direct synthesis of DME from CO_2 by combining a methanol synthesis catalyst and a solid acid catalyst, and found that a physical mixture (also known as a hybrid catalyst) of $Cu–ZnO–ZrO_2$ and H-ZSM-5 gave the highest oxygenate (CH_3OH + DME) productivity. Higher oxygenate productivity was also observed for a Pd/ZnO–ZSM-5 hybrid catalyst compared to a PdZn on ZSM-5 catalyst.[38] Ihm *et al.*[39] reported the direct synthesis of hydrocarbons from $CO_2 + H_2$ on $CuO/ZnO/ZrO_2$–ZSM-5 (Si/Al = 22) hybrid catalysts. At 400 °C and 30

bar the selectivity towards CO, oxygenates and hydrocarbons observed was 93.4, 1.8 and 4.8% respectively. C_{5+} products were detected, although C_1 and C_2 products accounted for 95.4% of the hydrocarbon product distribution. Over a $ZnZrO_2$/SAPO catalyst at 380 °C and 20 bar (~18% CO_2 conversion), the CO selectivity was reduced to 47%, whilst C_2–C_4 olefins accounted for 80% of the total hydrocarbon distribution, and the remaining hydrocarbons were assigned to C_2–C_4 alkanes (14%), C_1 (3%) and C_{5+} (3%).[40] Light olefins synthesised on hybrid catalysts from CO_2 can also undergo further reduction to their corresponding alkanes on the methanol synthesis catalyst, which effectively acts as a hydrogenation catalyst. Park *et al.*[41] reported ethane (76.4%) as the main hydrocarbon product over a $CuZnOZrO_2$–ZSM-5 catalyst (28 bar, 400 °C), with little formation of C_3 (4.5%), C_4 (0.8%) and C_{5+} (0.2%) products. However, as reported by Giordano, Frusteri and co-workers[42,43] for CO_2 conversion to DME over CuZnZr/ferrierite hybrid catalysts, Cu remains prone to severe sintering under the reaction conditions (260 °C, 30 bar). This makes catalyst stability the bottle neck of this process.

To the best of our knowledge, reports on PdZn hybrid catalysts for CO_2 hydrogenation focus on DME,[27,38] but no detailed attention has been paid to the produced hydrocarbons. We therefore assessed the activity and stability of diverse $PdZn/TiO_2$–ZSM-5 hybrid catalysts under CO_2 hydrogenation conditions (20 bar, <360 °C) and identified produced hydrocarbons derived from MTH and DMTH.

Experimental section

Materials

All ZSM-5 zeolites used in this work were purchased from Alfa Aesar (NH_4^+-form of ZSM-5, Si/Al = 23, 50 and 80); Pd acetylacetonate ($Pd(acac)_2$, 99%) and Zn acetylacetonate ($Zn(acac)_2$, 99%) were supplied by Sigma-Aldrich; titanium oxide (TiO_2-P25) was ordered from Aeroxide.

$PdZn/TiO_2$ catalyst synthesis

The synthesis of $PdZn/TiO_2$ by chemical vapour impregnation (CVI) was reported previously.[25–27] For the synthesis of 3 g of $PdZn/TiO_2$ catalyst with a 5 wt% Pd loading and a 1 : 5 palladium to zinc molar ratio, $Pd(acac)_2$ (0.43 g, 1.40 mmol), $Zn(acac)_2$ (2.06 g, 6.93 mmol) and TiO_2 (2.39 g) were physically mixed in a glass vial until homogeneous. The mixture was then transferred into a Schlenk flask, evacuated (10^{-3} bar) and heated (145 °C, 1 h). The as prepared materials were recovered and annealed in static air (10 °C min^{-1}, 500 °C, 16 h). $PdZn/TiO_2$ characterisation was performed on a portion of catalyst reduced in flowing 5% H_2/Ar (400 °C, 5 °C min^{-1}, 1 h).

$PdZn/TiO_2$–ZSM-5 hybrid catalyst preparation

The as received (NH_4)–ZSM-5 zeolites were annealed in static air (550 °C, 10 °C min^{-1}, 6 h) to obtain the H-ZSM-5 form prior to reaction. 0.5 g of $PdZn/TiO_2$ and 0.5 g of treated ZSM-5 were physically mixed in a vial until homogeneous. The mixture was pelleted (10 ton) and crushed (425–600 μm) to obtain the hybrid catalyst. Zeolites are named in the text according to their Si/Al ratio, for instance ZSM-5 with a Si/Al ratio of 23 : 1 will be referred to as ZSM-5(23).

CO_2 hydrogenation and consecutive MTH/DMTH catalyst testing

Catalytic activity for CO_2 hydrogenation to CH_3OH, DME, olefins and hydrocarbons was achieved in a stainless steel fixed-bed (50 cm length, 0.5 cm internal diameter) continuous flow reactor. 0.5 g of hybrid catalyst without diluent (or 0.25 g of pelleted $PdZn/TiO_2$ with 0.25 g of SiC as diluent) were secured in the reactor tube using quartz wool. Prior to reaction, the hybrid catalysts were pre-reduced in 5% H_2/He (400 °C, 5 °C min^{-1}, 1 h). Subsequently, the reactor was cooled down to 50 °C, the 5% H_2/He flow was switched to the reaction mixture ($CO_2/N_2/H_2 = 1:1:3$, 30 ml min^{-1}), and the reactor was pressurised to 20 bar and heated to the desired reaction temperature (240, 270, 300, 320, 340 and 360 °C, 5 °C min^{-1}, 6 h dwell). To avoid product condensation, post reactor lines and valves were heated to 130 °C. Products were analysed *via* online gas chromatography (Agilent 7890, fitted with FID and TCD detectors). Details of how CO_2 conversion, product selectivity and productivities were calculated can be found in the ESI (eqn (S1–S11†)).

Catalyst characterisation

X-ray absorption spectroscopy (XAS) was carried out in transmission mode at the Pd K-edge, at the B18 beamline of the Diamond Light Source, Harwell, UK, and a Pd foil was examined simultaneously with the sample and used as a reference. Three spectra were averaged to minimise the noise signal. The X-ray absorption fine structure (EXAFS) was analysed with the Demeter software package (Athena and Artemis).[44] X-ray photoelectron spectroscopy (XPS) was carried out on a Kratos Axis Ultra-DLD fitted with a monochromatic Al Kα (75–150 W) source and analyser, using a pass energy of 40 eV. The XPS data were analysed using Casa XPS software. Powder X-ray diffraction (XRD) patterns were obtained on a (θ–θ) PANalytical X'pert Pro powder diffractometer fitted with a hemispherical analyser using a Cu Kα radiation source (40 keV, 40 mA). The pore sizes and BET surface areas of the ZSM-5 zeolites were obtained through N_2 adsorption isotherms using a 3-flex Micromeritics instrument. Samples were degassed *in situ* at 250 °C for 10 h prior to analysis. Coke deposition during CO_2 hydrogenation was measured through thermogravimetric analysis on a PerkinElmer TL9000 with a TG-IR-MS interface.

Results and discussion

$PdZn/TiO_2$–ZSM-5 hybrid catalysts for direct CO_2 conversion to hydrocarbons

In addition to $PdZn/TiO_2$ employed as a CH_3OH synthesis catalyst,[20–23] commercial ZSM-5 zeolites with various Si/Al ratios (23, 50 and 80) were used as solid acid catalysts to promote consecutive CH_3OH dehydration to DME[27–30] and further MTH/DMTH.[32–34] XRD patterns, pore sizes and BET surface areas for the commercial ZSM-5 zeolites after annealing (static air, 550 °C, 10 °C min^{-1}, 6 h) can be found in the ESI (Fig. S1 and Table S1,† respectively). Thorough characterisation of $PdZn/TiO_2$ synthesised by chemical vapour impregnation (CVI) with 5 wt% Pd and a Pd/Zn molar ratio of 1 : 5 was previously reported.[25–27]

Firstly, the catalytic activity of $PdZn/TiO_2$ (0.25 g catalyst diluted with 0.25 g of SiC) for CO_2 hydrogenation was assessed (20 bar, $CO_2/N_2/H_2 = 1:1:3$, 240–360 °C). As observed in Table S2,† raising the reaction temperature from 240 to

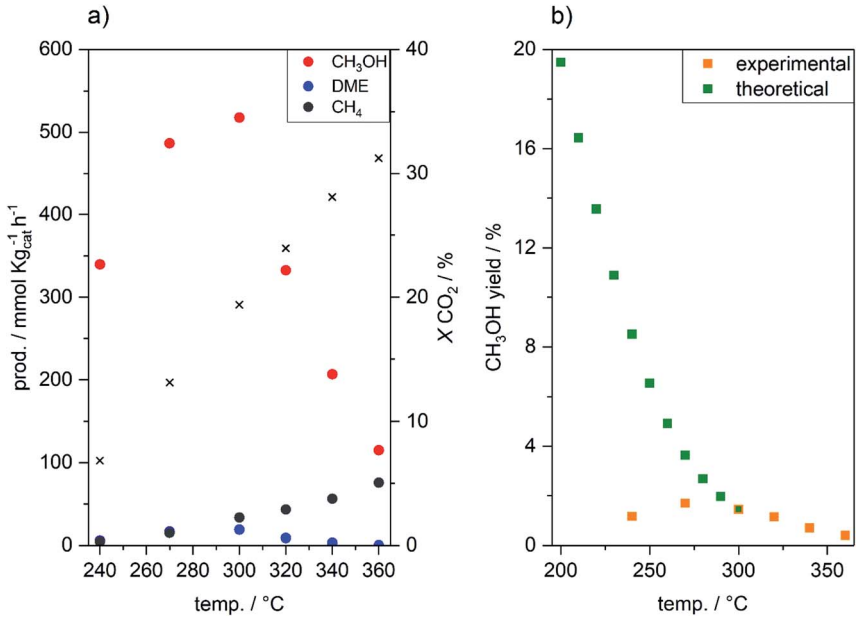

Fig. 1 (a) CH_3OH, DME and CH_4 productivities and CO_2 conversion for CO_2 hydrogenation (20 bar, 30 ml min^{-1}, $CO_2/H_2/N_2 = 1:3:1$, 240–360 °C, 6 h dwell) over $PdZn/TiO_2$. (b) Theoretical CH_3OH yield obtained from Shen *et al.*[45] compared to experimental CH_3OH yield with temperature over $PdZn/TiO_2$.

360 °C resulted in an increase in the CO_2 conversion from 6.8 to 31.2%, accompanied by an increase in the CO selectivity (from 74.6 to 97.9%) at the expense of CH_3OH selectivity (from 24.3 to 1.3%), in accordance with the reaction thermodynamics.[45] Below 300 °C, CH_3OH synthesis proceeded in the kinetic regime (Fig. 1a), as shown by the increase in the CH_3OH productivity with temperature up to 518 mmol kg_{cat}^{-1} h^{-1}. At 300 °C, the CH_3OH yield reached equilibrium (1.45% CH_3OH yield),[45] and hence, above 300 °C CH_3OH synthesis is controlled by the thermodynamic equilibrium (Fig. 1b), as shown by the sharp decrease in CH_3OH productivity. Low selectivity toward CH_4 (<0.8%) and DME (<1.0%), produced by CH_3OH decomposition on TiO_2 (ref. 46 and 47) and CH_3OH dehydration,[27] respectively, was observed. Nevertheless, in the absence of ZSM-5 solid acid catalysts, no other hydrocarbons were detected.

Comparable CO_2 conversion and CO productivity to $PdZn/TiO_2$ were observed for all $PdZn/TiO_2$–ZSM-5 hybrid catalysts (Fig. 2), indicating that the activity of the methanol synthesis catalyst is not altered by the proximity of solid acid zeolites, and that ZSM-5 zeolites are not active towards the RWGS. To ensure that ZSM-5 zeolites do not act as RWGS or as CH_3OH synthesis catalysts, blank ZSM-5(23) was employed for the CO_2 hydrogenation reaction (Table S3†), and negligible CO_2 conversion was observed at 270 °C. The efficient dehydration of CH_3OH to DME occurred over all $PdZn/TiO_2$–ZSM-5 hybrid catalysts. The highest oxygenate productivity (CH_3OH + DME) was obtained at 270 °C. At this temperature almost no methanol to olefins (MTH) or dimethyl ether to olefins (DMTH) conversion takes place, with only small traces of ethane detected over hybrid catalysts with

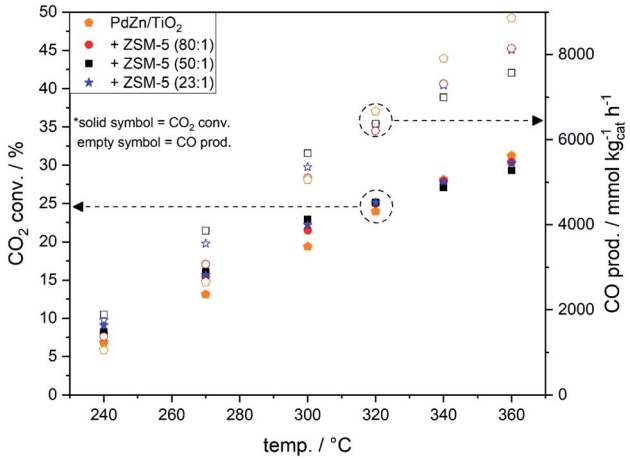

Fig. 2 CO_2 conversion and CO productivity over PdZn/TiO_2 and PdZn/TiO_2–ZSM-5 hybrid catalysts during CO_2 hydrogenation (20 bar, 30 ml min^{-1}, $CO_2/H_2/N_2 = 1:3:1$, 240–360 °C, 6 h dwell).

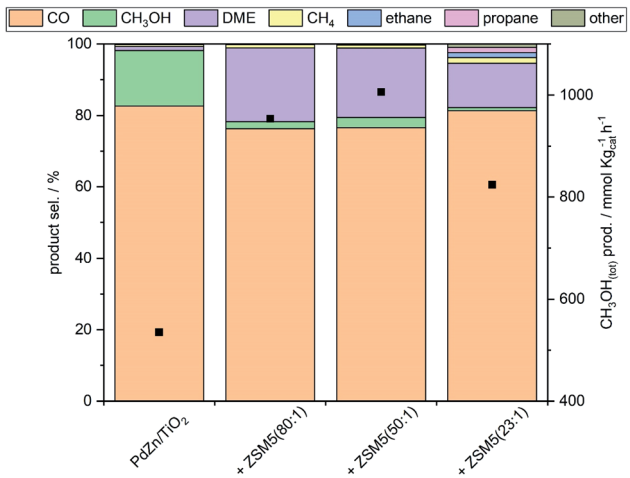

Fig. 3 CO, oxygenate and hydrocarbon selectivity and total CH_3OH productivity for CO_2 hydrogenation (20 bar, 270 °C, $CO_2/H_2/N_2 = 1:3:1$) over PdZn/TiO_2 and PdZn/TiO_2–ZSM-5 hybrid catalysts.

ZSM-5(50 and 80), and small amounts of higher hydrocarbons observed for PdZn/TiO_2–ZSM-5(23). DME is the major oxygenate product with a selectivity close to 20%. Moreover, the total methanol productivity ($CH_3OH_{(tot)}$), considering that all hydrocarbons originate from CH_3OH by either dehydration to DME or through the MTH/DMTH process, was higher for all hybrid catalysts compared to PdZn/TiO_2 (Fig. 3).

The hydrocarbon productivities and $CH_3OH_{(tot)}$ over PdZn/TiO_2–ZSM-5 hybrid catalysts can be found in Table S4.† At 300 °C, the hybrid catalysts showed higher

$CH_3OH_{(tot)}$ compared to $PdZn/TiO_2$, thus overcoming the theoretical CH_3OH yield dictated by the equilibrium. Increasing the alumina ratio in the zeolite promoted the formation of longer hydrocarbons. The presence of aluminium sites is related to Brønsted acid sites with mild acidity, and hence, a higher concentration of Brønsted acid sites promotes chain growth *via* the hydrocarbon pool mechanism.[33,48] Light olefins produced as intermediates in MTH[49] undergo further hydrogenation over $PdZn/TiO_2$, yielding the corresponding alkanes (ethane and propane); a mixture of *n*-butane and 2-butene was observed, whilst only olefins were detected in the C_5 fraction (1-pentene and 2-*cis*/*trans*-pentene). Thus, when PdZn alloys are used for the synthesis of hydrocarbons from CO_2 *via* a methanol mediated route over hybrid catalysts, they behave as methanol synthesis catalysts but also as olefin hydrogenation catalysts, limiting hydrocarbon chain growth as also reported for Cu-based catalysts.[49–51] $CH_3OH_{(tot)}$ over hybrid catalysts is higher compared to $PdZn/TiO_2$ at any temperature, with total CH_3OH productivity surpassing the equilibrium yield above 300 °C. The highest total CH_3OH productivity for hybrid catalysts was observed in the 270–300 °C range; hybrid catalysts with ZSM-5(80 and 50) gave the highest oxygenate productivity (CH_3OH and DME), while ZSM-5(23) led to higher hydrocarbon productivity (Fig. 4) *via* faster MTH/DMTH. Although the total CH_3OH productivity was higher than the equilibrium yield, above 300 °C, the hydrocarbon productivity is limited by CH_3OH availability which leads to a decrease in the total CH_3OH productivity at higher temperatures. The hydrocarbon selectivity based on MTH/DMTH showed that increasing the aluminium concentration in ZSM-5 in the hybrid catalyst resulted in improved selectivity towards higher hydrocarbons (Table S5†). In the 320–340 °C temperature range ethane and propane accounted for 50% of MTH/DMTH product selectivity for all hybrid catalysts. Note that the real CH_4

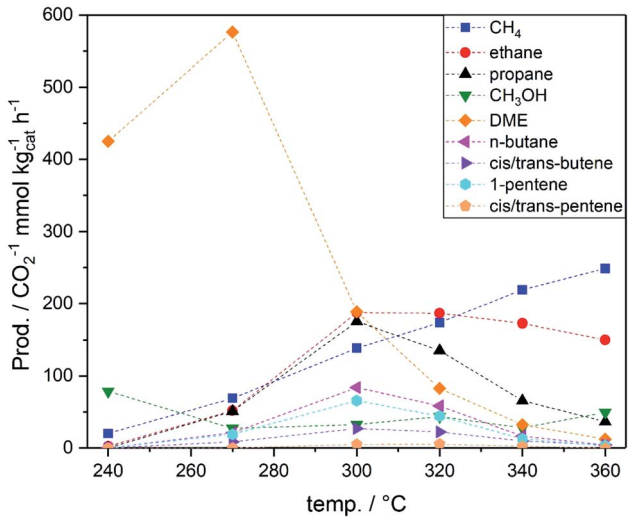

Fig. 4 Productivities based on carbon (*e.g.*, two molecules of CO_2 converted per ethane molecule and three molecules of CO_2 converted per propane molecule) during CO_2 hydrogenation (20 bar, 30 ml min^{-1}, $CO_2/H_2/N_2 = 1:3:1$) over the $PdZn/TiO_2$–ZSM-5(23) hybrid catalyst.

selectivity *via* the MTH and DMTH process is lower than the reported values, since CH_4 is also produced as a by-product in CH_3OH decomposition on $PdZn/TiO_2$.[47]

Catalytic stability of $PdZn/TiO_2$ under the reaction conditions

The higher stability of PdZn alloy catalysts compared to their Cu-based counterparts was proven under methanol reforming conditions,[15,52–54] which is the opposite reaction to the intended CO_2 hydrogenation to CH_3OH. Copper sinters in the presence of water at elevated temperatures, and hence, due to the higher water content when the feed is CO_2 instead of CO, PdZn alloys are employed as stable alternatives to Cu-based catalysts for the synthesis of CH_3OH from CO_2.[15–19] According to the Pd–Zn phase diagram developed by Massalski[55] and Vizdal *et al.*,[56] the β-PdZn alloy is thermally stable up to 1200 °C. However, in the presence of oxygen at 300 °C, the surface of the PdZn alloy segregates into ZnO and metallic Pd,[53] whilst under H_2, the β-PdZn alloy was experimentally proven to be stable up to 600 °C.[57] Chen *et al.*,[58] based on DFT calculations, suggested that Zn segregates from the PdZn alloy when the alloy is supported on ZnO. Nevertheless, Ahoba-Sam *et al.*[38] reported no changes in the PdZn phase and no formation of extra Pd-phases through *operando* XAS during CO_2 hydrogenation to CH_3OH (8 bar, 350 °C).

The stability of the PdZn phase in the $PdZn/TiO_2$ methanol synthesis catalyst was assessed through XAS, XRD and XPS characterisation pre- and post-reaction

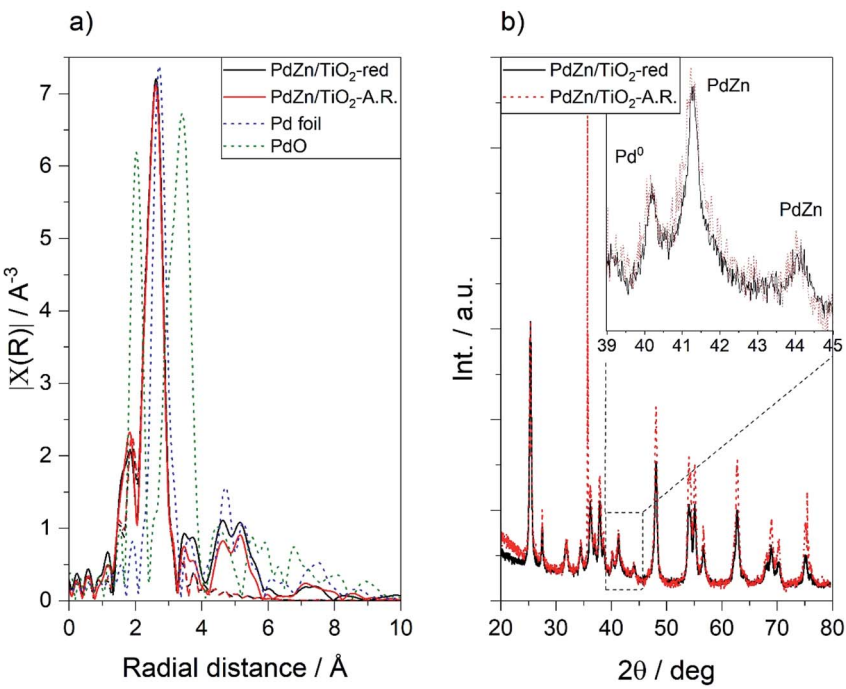

Fig. 5 (a) EXAFS spectra of $PdZn/TiO_2$ after reduction and $PdZn/TiO_2$ after reaction (240–360 °C). Recorded spectra and fits (window 1.8–3.5 Å) are represented by solid and dashed lines, respectively. Spectra of Pd foil and PdO are included for comparison; (b) XRD patterns recorded for $PdZn/TiO_2$ after reduction and $PdZn/TiO_2$ after reaction.

(20 bar, $CO_2/H_2/N_2 = 1:3:1$, 30 ml min^{-1}, 240–360 °C, 6 h dwell, 36 h reaction). Extended X-ray absorption fine-structure spectroscopy (EXAFS) at the Pd K-edge was employed to detect structural and electronic changes in the PdZn phase after reaction. No noticeable differences were observed between the EXAFS spectra up to 3.5 Å of $PdZn/TiO_2$ after pre-reduction (5% H_2, 400 °C, 1 h) and after CO_2 hydrogenation at up to 360 °C (Fig. 5a). Bulk Pd has a cubic structure with a Pd–Pd bond distance of 1.75 Å, whilst the β-PdZn alloy has a tetragonal structure. As expected for the intercalation of a Zn atom between two Pd atoms, on average shorter bond distances for the first coordination shell compared to bulk Pd were observed (shorter Pd–Zn bond distance compared to the Pd–Pd distance in Pd foil).[59] Moreover, comparison with a PdO standard could suggest the presence of a Pd–O bond at 2.02 Å, with the concomitant but lower intensity Pd–O–Pd bond at 3.41 Å in the second coordination shell.[60] This could be attributed to oxidation of the first atomic layer of the PdZn alloy in contact with air.[53] Peak fitting using Artemis[44] allowed us to obtain the Pd–Pd and Pd–Zn bond distances and the Pd coordination environment (Table 1). Details of the fitting can be obtained from Table S6.† Based on previous reports, PdZn alloy formation begins at the surface of Pd nanoparticles *via* hydrogen spillover to adjacent ZnO, and the alloy grows inwards, generating a PdZn layer over a Pd core.[53,57] Therefore, the incorporation of bulk Pd–Pd bond distances was necessary to obtain a good fit. No differences in the Pd–Zn or Pd–Pd bond distances or coordination number were observed, suggesting high bulk structural stability of the PdZn alloy under reaction conditions, as also reported by Olsbye and co-workers.[38] Despite the apparent bond distance at 2.02 Å, no good fit was obtained after the introduction of the Pd–O scattering path, indicating that this contribution can be attributed to noise or to marginal PdO content.

Phase changes in the β-PdZn alloy during reaction were investigated by recording the XRD pattern of $PdZn/TiO_2$ after reduction (400 °C, 1 h) and after reaction (240–360 °C, 20 bar, 36 h). In agreement with the EXAFS analysis, no changes were observed in the (111) and (200) β-PdZn reflections at 41.2° and 44.1° respectively,[15,19,27] showing the high thermal stability of bulk PdZn under the reaction conditions (Fig. 5b). Moreover, no significant changes were observed in the XRD peak at 40.1° assigned to metallic Pd (PDF 00-046-1043), which presumably is protected underneath a PdZn layer.[53,57] Unincorporated Zn in the

Table 1 Bond distances and coordination numbers for $PdZn/TiO_2$ after reduction and $PdZn/TiO_2$ after reaction obtained from EXAFS fitting

$PdZn/TiO_2$	Bond	Distance	CN	σ^2	R_f
Reduced	$Pd–Zn_{(alloy)}$	2.59	2.62–0.21	0.0047–0.0014	0.019
	$Pd–Pd_{1(alloy)}$	3.06	7.58	0.0217–0.0055	
	$Pd–Pd_{2(alloy)}$	3.35	3.79	0.0215–0.0111	
	$Pd–Pd_{(metal)}$	2.75	12 (fixed)	0.0238–0.0030	
A.R.	$Pd–Zn_{(alloy)}$	2.60	2.71	0.0050–0.0015	0.020
	$Pd–Pd_{1(alloy)}$	3.03	7.52	0.0216–0.0068	
	$Pd–Pd_{2(alloy)}$	3.31	3.76–0.2	0.0218–0.0115	
	$Pd–Pd_{(metal)}$	2.74	12 (fixed)	0.0220–0.0030	
Pd foil	$Pd–Pd_1$	2.75	12 (fixed)	0.0055–0.0002	0.016
	$Pd–Pd_2$	3.89	6 (fixed)	0.0097–0.0022	

PdZn alloy is observed as ZnO at 31.7°, 34.4° and 36.3° (PDF 00-036-1451). In line with PdZn and Pd, no changes in the ZnO reflections were observed after reaction. Nevertheless, the TiO_2-related reflections become more intense after reaction, suggesting an increase in the particle size of the support (Fig. S2†).

EXAFS and XRD are averaging techniques sensitive to bulk changes. Catalysis, however, is a surface process, and hence small changes at the surface greatly affect the catalytic activity. To follow surface changes in the PdZn alloy composition, the Pd(3d) and Zn(LM_2) orbitals of the PdZn/TiO_2 catalyst before and after reaction were analysed by X-ray photoelectron spectroscopy (XPS). The Zn(2p) orbital is not sensitive towards chemical changes (*e.g.* the binding energies for Zn^0 and Zn^{2+} are reported at 1021.7 and 1022 eV, respectively),[61] and as observed by XRD, the unalloyed zinc remained as ZnO, hence the Pd(3d) and Zn(LM_2) orbitals were calibrated against the Zn(2p) orbital at 1022 eV. The Pd(3d) peak for PdZn/TiO_2 after reduction and after reaction was centred at 335.6 eV (Fig. 6), between the binding energy values reported for metallic Pd (334.8–335.4 eV)[62–64] and the PdZn alloy (335.6–336.7 eV).[64–66] Peak fitting using finite Lorentzian line shapes for the Pd and PdZn peaks (including satellites) and Gaussian line shapes for the PdO peaks and satellites with a Shirley background as described previously[47] indicated the presence of Pd, PdZn and PdO at 335.0, 335.9 and 337.2 eV, respectively (Fig. S3a†).[54,64] The presence of Pd and PdZn was confirmed by the XRD and EXAFS bulk characterisation techniques, however bulk PdO was not observed. The broadening of the Pd(3d) peak after reaction indicated an increase in the proportion of surface PdO, suggesting that surface PdZn phase separation into ZnO and Pd occurred, with concomitant palladium passivation when in contact with air.[53] No significant changes were observed in the Zn(LM_2) Auger electron spectra before and after reaction (Fig. S3b†); the main peak at 998 eV with a minor satellite contribution at 991 eV was attributed to the presence of ZnO.[67]

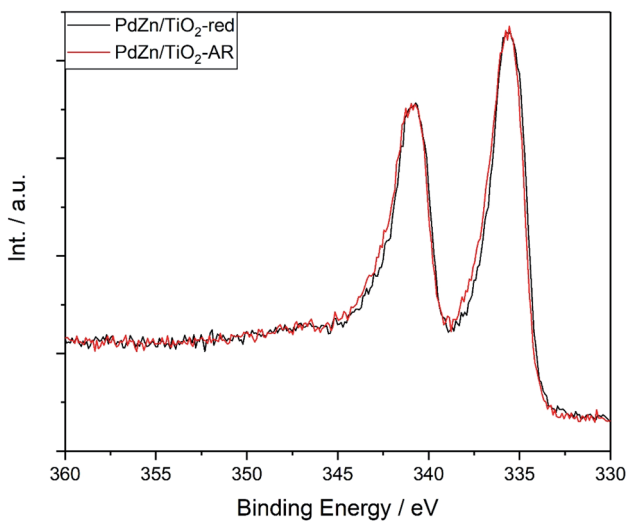

Fig. 6 Pd(3d) XPS analysis for PdZn/TiO_2 after reduction (5% H_2, 400 °C, 1 h) and after reaction (20 bar, 240–360 °C, 36 h, $CO_2 : H_2 : N_2 = 1 : 3 : 1$).

No significant changes in the PdZn phase were detected by EXAFS or XRD, confirming the bulk thermal stability of PdZn under reaction conditions (20 bar, 240–340 °C, $CO_2/H_2/N_2 = 1:3:1$, 36 h). However some surface PdZn phase separation into Pd and ZnO was suggested by the XPS characterisation. Coke deposition is often reported as the main deactivation mechanism for MTH over acid zeolite catalysts. Coke inhibits CH_3OH diffusion to the acid active sites by either filling zeolite cavities or blocking pores.[34] Zeolites can be regenerated at high temperature (500–600 °C) by oxidising deposited coke to CO_2 with oxygen.[68] To assess the extent of coke deposition during CO_2 hydrogenation (20 bar, 240–340 °C, $CO_2/H_2/N_2 = 1:3:1$, 36 h) over PdZn/TiO_2–ZSM-5 hybrid catalysts, TGA-MS was performed on fresh and spent catalysts (Fig. S4†). The mass loss observed below 200 °C can be assigned to physi/chemisorbed water. Just above 200 °C, an extra 1 wt% mass loss compared to the fresh samples was observed for the PdZn/TiO_2–ZSM-5(80 and 50) hybrid catalysts with a corresponding release of CO_2, which could be assigned to coke deposits with high oxygen content as reported for CH_3OH conversion to olefins over ZSM-5.[69] No additional mass loss at higher temperature, which would be assigned to coke deposits with low oxygen and hydrogen content (*e.g.* aromatics), was detected.[69] No coke deposition was detected for PdZn/TiO_2–ZSM-5(23). This should not be interpreted as ZSM-5(23) being less sensitive to coke deposition, since a higher concentration of acid sites generally leads to faster deactivation,[70] but instead the initial rate of coke formation might be slower in this system. This might be attributed to the presence of H_2O and H_2 in the feed[35–37] as well as the low concentration of CH_3OH throughout the catalyst bed.[69]

Conclusions

The combination of a PdZn/TiO_2 methanol synthesis catalyst with solid acid ZSM-5 zeolites in the form of a hybrid catalyst allowed for consecutive CO_2 hydrogenation to CH_3OH, CH_3OH dehydration to DME, and MTH/DMTH in a one-pass single bed reactor. Thus, the total CH_3OH productivity from CO_2 hydrogenation over PdZn/TiO_2–ZSM-5 hybrid catalysts was higher compared to PdZn/TiO_2. The synthesised light olefins undergo further hydrogenation to the corresponding alkanes (ethane, propane and butane) as also reported for Cu-based catalysts, which limit hydrocarbon chain growth. Hence, future research using PdZn alloys for the synthesis of hydrocarbons *via* the methanol route should focus on limiting the activity towards olefin hydrogenation whilst maintaining good selectivity for CH_3OH. Increasing the concentration of aluminium sites in ZSM-5, correlated with mild Brønsted acid sites, resulted in the production of higher hydrocarbons. The bulk stability of the PdZn/TiO_2 catalyst up to 360 °C under the reaction conditions (20 bar, $CO_2/H_2/N_2 = 1:3:1$, 30 ml min^{-1}, 36 h) was confirmed by XAS and XRD. However XPS suggests that some surface PdZn separation into Pd and ZnO occurred during the reaction.

Dataset available

Data information can be found at http://doi.org/10.17035/d.2021.0129194354.

Conflicts of interest

There are no conflicts to declare.

Acknowledgements

The authors would like to acknowledge the UK Catalysis Hub and the EPSRC for funding (EP/N010531/1) the presented research. We would like to thank Dr Greg Shaw for helping us with TGA-MS measurements.

References

1 J. Rockström, W. Steffen, K. Noone, Å. Persson, F. S. Chapin III, E. F. Lambin, T. M. Lenton, M. Scheffer, C. Folke, H. J. Schellnhuber, B. Nykvist, C. A. de Wit, T. Hughes, S. van der Leeuw, H. Rodhe, S. Sörlin, P. K. Snyder, R. Costanza, U. Svedin, M. Falkenmark, L. Karlberg, R. W. Corell, V. J. Fabry, J. Hansen, B. Walker, D. Liverman, K. Richardson, P. Crutzen and J. A. Foley, A Safe Operating Space for Humanity, *Nature*, 2009, **461**, 472.

2 J. Twidel, *Renewable Energy Sources*, Routledge, 2015.

3 R. Schlögl, The Role of Chemistry in the Energy Challenge, *ChemSusChem*, 2010, **3**(2), 209–222.

4 M. Carmo, D. L. Fritz, J. Mergel and D. Stolten, A Comprehensive Review on PEM Water Electrolysis, *Int. J. Hydrogen Energy*, 2013, **38**(12), 4901–4934.

5 P. C. Ghosh, B. Emonts, H. Janßen, J. Mergel and D. Stolten, Ten Years of Operational Experience with a Hydrogen-Based Renewable Energy Supply System, *Sol. Energy*, 2003, **75**(6), 469–478.

6 A. Ursua, L. M. Gandia and P. Sanchis, Hydrogen Production From Water Electrolysis: Current Status and Future Trends, *Proc. IEEE*, 2012, **100**(2), 410–426.

7 DECHEMA Technology Roadmap, *Energy and GHG Reductions in the Chemical Industry via Catalytic Processes*, International Energy Agency, 2018.

8 M. Bowker, Methanol Synthesis from CO_2 Hydrogenation, *ChemCatChem*, 2019, **11**, 4238–4246.

9 E. V. Kondratenko, G. Mul, J. Baltrusaitis, G. O. Larrazábal and J. Pérez-Ramírez, Status and Perspectives of CO_2 Conversion into Fuels and Chemicals by Catalytic, Photocatalytic and Electrocatalytic Processes, *Energy Environ. Sci.*, 2013, **6**(11), 3112–3135.

10 S. G. Jadhav, P. D. Vaidya, B. M. Bhanage and J. B. Joshi, Catalytic Carbon Dioxide Hydrogenation to Methanol: A Review of Recent Studies, *Chem. Eng. Res. Des.*, 2014, **92**(11), 2557–2567.

11 H. Yang, C. Zhang, P. Gao, H. Wang, X. Li, L. Zhong, W. Wei and Y. Sun, A Review of the Catalytic Hydrogenation of Carbon Dioxide into Value-Added Hydrocarbons, *Catal. Sci. Technol.*, 2017, **7**(20), 4580–4598.

12 J. Ma, N. Sun, X. Zhang, N. Zhao, F. Xiao, W. Wei and Y. Sun, A Short Review of Catalysis for CO_2 Conversion, *Catal. Today*, 2009, **148**(3–4), 221–231.

13 M. B. Fichtl, D. Schlereth, N. Jacobsen, I. Kasatkin, J. Schumann, M. Behrens, R. Schlögl and O. Hinrichsen, Kinetics of Deactivation on $Cu/ZnO/Al_2O_3$ Methanol Synthesis Catalysts, *Appl. Catal., A*, 2015, **502**, 262–270.

14 J. Ereña, I. Sierra, M. Olazar, A. G. Gayubo and A. T. Aguayo, Deactivation of a $CuO–ZnO–Al_2O_3/\gamma\text{-}Al_2O_3$ Catalyst in the Synthesis of Dimethyl Ether, *Ind. Eng. Chem. Res.*, 2008, **47**(7), 2238–2247.

15 T. Conant, A. M. Karim, V. Lebarbier, Y. Wang, F. Girgsdies, R. Schlögl and A. Datye, Stability of Bimetallic Pd–Zn Catalysts for the Steam Reforming of Methanol, *J. Catal.*, 2008, **257**(1), 64–70.

16 C.-H. Kim, J. S. Lee and D. L. Trimm, The Preparation and Characterisation of Pd–ZnO Catalysts for Methanol Synthesis, *Top. Catal.*, 2003, **22**(3), 319–324.
17 L. Fan and K. Fujimoto, Promotive SMSI Effect for Hydrogenation of Carbon Dioxide to Methanol on a Pd/CeO_2 Catalyst, *J. Catal.*, 1994, **150**(1), 217–220.
18 A. S. Malik, S. F. Zaman, A. A. Al-Zahrani, M. A. Daous, H. Driss and L. A. Petrov, Development of Highly Selective PdZn/CeO_2 and Ca-Doped PdZn/CeO_2 Catalysts for Methanol Synthesis from CO_2 Hydrogenation, *Appl. Catal., A*, 2018, **560**, 42–53.
19 J. Xu, X. Su, X. Liu, X. Pan, G. Pei, Y. Huang, X. Wang, T. Zhang and H. Geng, Methanol Synthesis from CO_2 and H_2 over Pd/ZnO/Al_2O_3: Catalyst Structure Dependence of Methanol Selectivity, *Appl. Catal., A*, 2016, **514**, 51–59.
20 N. Iwasa, H. Suzuki, M. Terashita, M. Arai and N. Takezawa, Methanol Synthesis from CO_2 Under Atmospheric Pressure over Supported Pd Catalysts, *Catal. Lett.*, 2004, **96**(1), 75–78.
21 H. Bahruji, M. Bowker, G. Hutchings, N. Dimitratos, P. Wells, E. Gibson, W. Jones, C. Brookes, D. Morgan and G. Lalev, Pd/ZnO Catalysts for Direct CO_2 Hydrogenation to Methanol, *J. Catal.*, 2016, **343**, 133–146.
22 J. Díez-Ramírez, P. Sánchez, A. Rodríguez-Gómez, J. L. Valverde and F. Dorado, Carbon Nanofiber-Based Palladium/Zinc Catalysts for the Hydrogenation of Carbon Dioxide to Methanol at Atmospheric Pressure, *Ind. Eng. Chem. Res.*, 2016, **55**(12), 3556–3567.
23 J. Díez-Ramírez, F. Dorado, A. R. de la Osa, J. L. Valverde and P. Sánchez, Hydrogenation of CO_2 to Methanol at Atmospheric Pressure over Cu/ZnO Catalysts: Influence of the Calcination, Reduction, and Metal Loading, *Ind. Eng. Chem. Res.*, 2017, **56**(8), 1979–1987.
24 X.-L. Liang, X. Dong, G.-D. Lin and H.-B. Zhang, Carbon Nanotube-Supported Pd–ZnO Catalyst for Hydrogenation of CO_2 to Methanol, *Appl. Catal., B*, 2009, **88**(3–4), 315–322.
25 H. Bahruji, M. Bowker, W. Jones, J. Hayward, J. Ruiz Esquius, D. J. Morgan and G. J. Hutchings, PdZn Catalysts for CO_2 Hydrogenation to Methanol Using Chemical Vapour Impregnation (CVI), *Faraday Discuss.*, 2017, **197**, 309–324.
26 H. Bahruji, J. R. Esquius, M. Bowker, G. Hutchings, R. D. Armstrong and W. Jones, Solvent Free Synthesis of PdZn/TiO_2 Catalysts for the Hydrogenation of CO_2 to Methanol, *Top. Catal.*, 2018, **61**(3), 144–153.
27 H. Bahruji, R. D. Armstrong, J. R. Esquius, W. Jones, M. Bowker and G. J. Hutchings, Hydrogenation of CO_2 to Dimethyl Ether over Brønsted Acidic PdZn Catalysts, *Ind. Eng. Chem. Res.*, 2018, **57**(20), 6821–6829.
28 A. Álvarez, A. Bansode, A. Urakawa, A. V. Bavykina, T. A. Wezendonk, M. Makkee, J. Gascon and F. Kapteijn, Challenges in the Greener Production of Formates/Formic Acid, Methanol, and DME by Heterogeneously Catalyzed CO_2 Hydrogenation Processes, *Chem. Rev.*, 2017, **117**(14), 9804–9838.
29 G. Bonura, M. Cordaro, L. Spadaro, C. Cannilla, F. Arena and F. Frusteri, Hybrid Cu–ZnO–ZrO_2/H-ZSM5 System for the Direct Synthesis of DME by CO_2 Hydrogenation, *Appl. Catal., B*, 2013, **140–141**, 16–24.
30 S.-K. Ihm, S.-W. Baek, Y.-K. Park and J.-K. Jeon, CO_2 Hydrogenation over Copper-Based Hybrid Catalysts for the Synthesis of Oxygenates, in *Utilization of Greenhouse Gases;ACS Symposium Series*, American Chemical Society, 2003, vol. 852, pp. 183–194.

31 M. Xu, J. H. Lunsford, D. W. Goodman and A. Bhattacharyya, Synthesis of Dimethyl Ether (DME) from Methanol over Solid-Acid Catalysts, *Appl. Catal., A*, 1997, **149**(2), 289–301.
32 P. Tian, Y. Wei, M. Ye and Z. Liu, Methanol to Olefins (MTO): From Fundamentals to Commercialization, *ACS Catal.*, 2015, **5**(3), 1922–1938.
33 C. D. Chang, C. T.-W. Chu and R. F. Socha, Methanol Conversion to Olefins over ZSM-5: I. Effect of Temperature and Zeolite $SiO_2Al_2O_3$, *J. Catal.*, 1984, **86**(2), 289–296.
34 M. Stöcker, Methanol-to-Hydrocarbons: Catalytic Materials and Their Behavior, *Microporous Mesoporous Mater.*, 1999, **29**(1–2), 3–48.
35 S. S. Arora, Z. Shi and A. Bhan, Mechanistic Basis for Effects of High-Pressure H_2 Cofeeds on Methanol-to-Hydrocarbons Catalysis over Zeolites, *ACS Catal.*, 2019, **9**(7), 6407–6414.
36 S. S. Arora, D. L. S. Nieskens, A. Malek and A. Bhan, Lifetime Improvement in Methanol-to-Olefins Catalysis over Chabazite Materials by High-Pressure H_2 Co-Feeds, *Nat. Catal.*, 2018, **1**(9), 666–672.
37 X. Wu and R. G. Anthony, Effect of Feed Composition on Methanol Conversion to Light Olefins over SAPO-34, *Appl. Catal., A*, 2001, **218**(1–2), 241–250.
38 C. Ahoba-Sam, E. Borfecchia, A. Lazzarini, A. Bugaev, A. A. Isah, M. Taoufik, S. Bordiga and U. Olsbye, On the Conversion of CO_2 to Value Added Products over Composite PdZn and H-ZSM-5 Catalysts: Excess Zn over Pd, a Compromise or a Penalty?, *Catal. Sci. Technol.*, 2020, **10**, 4373–4385.
39 S.-K. Ihm, S.-W. Baek, Y.-K. Park and K.-C. Park, 24-P-26-The Nature of Medium Acidity in [CuO/ZnO/ZrO_2]SAPO-34 Hybrid Catalyst for CO_2 Hydrogenation: Study of the Interactions between Metal Oxides and Acid Sites in Zeolite, in *Studies in Surface Science and Catalysis*, ed. A. Galarneau, F. Fajula, F. Di Renzo and J. Vedrine, Elsevier, 2001, vol. 135, p. 277.
40 Z. Li, J. Wang, Y. Qu, H. Liu, C. Tang, S. Miao, Z. Feng, H. An and C. Li, Highly Selective Conversion of Carbon Dioxide to Lower Olefins, *ACS Catal.*, 2017, **7**(12), 8544–8548.
41 Y.-K. Park, K.-C. Park and S.-K. Ihm, Hydrocarbon Synthesis through CO_2 Hydrogenation over CuZnOZrO_2/Zeolite Hybrid Catalysts, *Catal. Today*, 1998, **44**(1–4), 165–173.
42 G. Bonura, M. Migliori, L. Frusteri, C. Cannilla, E. Catizzone, G. Giordano and F. Frusteri, Acidity Control of Zeolite Functionality on Activity and Stability of Hybrid Catalysts during DME Production via CO_2 Hydrogenation, *J. CO2 Util.*, 2018, **24**, 398–406.
43 I. Miletto, E. Catizzone, G. Bonura, C. Ivaldi, M. Migliori, E. Gianotti, L. Marchese, F. Frusteri and G. Giordano, In Situ FT-IR Characterization of CuZnZr/Ferrierite Hybrid Catalysts for One-Pot CO_2-to-DME Conversion, *Materials*, 2018, **11**, 2275–2289.
44 B. Ravel and M. Newville, ATHENA, ARTEMIS, HEPHAESTUS: Data Analysis for X-Ray Absorption Spectroscopy Using IFEFFIT, *J. Synchrotron Radiat.*, 2005, **12**(4), 537–541.
45 W.-J. Shen, K.-W. Jun, H.-S. Choi and K.-W. Lee, Thermodynamic Investigation of Methanol and Dimethyl Ether Synthesis from CO_2 Hydrogenation, *Korean J. Chem. Eng.*, 2000, **17**(2), 210–216.

46 H. Bahruji, M. Bowker, C. Brookes, P. R. Davies and I. Wawata, The Adsorption and Reaction of Alcohols on TiO_2 and Pd/TiO_2 Catalysts, *Appl. Catal., A*, 2013, **454**, 66–73.

47 J. Ruiz Esquius, H. Bahruji, S. H. Taylor, M. Bowker and G. J. Hutchings, CO_2 Hydrogenation to CH_3OH over PdZn Catalysts, with Reduced CH_4 Production, *ChemCatChem*, 2020, **12**, 6024–6032.

48 I. Yarulina, K. De Wispelaere, S. Bailleul, J. Goetze, M. Radersma, E. Abou-Hamad, I. Vollmer, M. Goesten, B. Mezari, E. J. M. Hensen, J. S. Martínez-Espín, M. Morten, S. Mitchell, J. Perez-Ramirez, U. Olsbye, B. M. Weckhuysen, V. Van Speybroeck, F. Kapteijn and J. Gascon, Structure–Performance Descriptors and the Role of Lewis Acidity in the Methanol-to-Propylene Process, *Nat. Chem.*, 2018, **10**(8), 804–812.

49 M. Fujiwara, R. Kieffer, H. Ando and Y. Souma, Development of Composite Catalysts Made of Cu-Zn-Cr Oxide/Zeolite for the Hydrogenation of Carbon Dioxide, *Appl. Catal., A*, 1995, **121**(1), 113–124.

50 M. Fujiwara, H. Ando, M. Tanaka and Y. Souma, Hydrogenation of Carbon Dioxide over Cu-Zn-Chromate/Zeolite Composite Catalyst: The Effects of Reaction Behavior of Alkenes on Hydrocarbon Synthesis, *Appl. Catal., A*, 1995, **130**(1), 105–116.

51 Y. Tan, M. Fujiwara, H. Ando, Q. Xu and Y. Souma, Selective Formation of Iso-Butane from Carbon Dioxide and Hydrogen over Composite Catalysts, in *Studies in Surface Science and Catalysis*, ed. T. Inui, M. Anpo, K. Izui, S. Yanagida and T. Yamaguchi, Elsevier, 1998, vol. 114, pp. 435–438.

52 R. A. Dagle, A. Platon, D. R. Palo, A. K. Datye, J. M. Vohs and Y. Wang, PdZnAl Catalysts for the Reactions of Water-Gas-Shift, Methanol Steam Reforming, and Reverse-Water-Gas-Shift, *Appl. Catal., A*, 2008, **342**(1–2), 63–68.

53 K. Föttinger, J. A. van Bokhoven, M. Nachtegaal and G. Rupprechter, Dynamic Structure of a Working Methanol Steam Reforming Catalyst: *In Situ* Quick-EXAFS on Pd/ZnO Nanoparticles, *J. Phys. Chem. Lett.*, 2011, **2**(5), 428–433.

54 N. Iwasa, S. Masuda, N. Ogawa and N. Takezawa, Steam Reforming of Methanol over Pd/ZnO: Effect of the Formation of PdZn Alloys upon the Reaction, *Appl. Catal., A*, 1995, **125**(1), 145–157.

55 T. B. Massalski, *Binary Alloy Phase Diagrams*, ASM International, Ohio, USA 1996.

56 J. Vizdal, A. Kroupa, J. Popovic and A. Zemanova, The Experimental and Theoretical Study of Phase Equilibria in the Pd–Zn (-Sn) System, *Adv. Eng. Mater.*, 2006, **8**(3), 164–176.

57 S. Penner, B. Jenewein, H. Gabasch, B. Klötzer, D. Wang, A. Knop-Gericke, R. Schlögl and K. Hayek, Growth and Structural Stability of Well-Ordered PdZn Alloy Nanoparticles, *J. Catal.*, 2006, **241**(1), 14–19.

58 Z.-X. Chen, K. M. Neyman and N. Rösch, Theoretical Study of Segregation of Zn and Pd in Pd–Zn Alloys, *Surf. Sci.*, 2004, **548**(1–3), 291–300.

59 Z.-X. Chen, K. M. Neyman, A. B. Gordienko and N. Rösch, Surface Structure and Stability of PdZn and PtZn Alloys: Density-Functional Slab Model Studies, *Phys. Rev. B*, 2003, **68**(7), 075417.

60 D. Cheng, K. Okumura, Y. Xie and C. Liu, Stability Test and EXAFS Characterization of Plasma Prepared Pd/HZSM-5 Catalyst for Methane Combustion, *Appl. Surf. Sci.*, 2007, **254**(5), 1506–1510.

61 https://xpssimplified.com/.

62 M. Brun, A. Berthet and J. C. Bertolini, XPS, AES and Auger Parameter of Pd and PdO, *J. Electron Spectrosc. Relat. Phenom.*, 1999, **104**(1–3), 55–60.
63 Y. Zhang, Y. Cai, Y. Guo, H. Wang, L. Wang, Y. Lou, Y. Guo, G. Lu and Y. Wang, The Effects of the Pd Chemical State on the Activity of Pd/Al_2O_3 Catalystsin CO Oxidation, *Catal. Sci. Technol.*, 2014, **4**(11), 3973–3980.
64 P. Kast, M. Friedrich, F. Girgsdies, J. Kröhnert, D. Teschner, T. Lunkenbein, M. Behrens and R. Schlögl, Strong Metal–Support Interaction and Alloying in Pd/ZnO Catalysts for CO Oxidation, *Catal. Today*, 2016, **260**, 21–31.
65 K. M. Eblagon, P. H. Concepción, H. Silva and A. Mendes, Ultraselective Low Temperature Steam Reforming of Methanol over PdZn/ZnO Catalysts—Influence of Induced Support Defects on Catalytic Performance, *Appl. Catal., B*, 2014, **154–155**, 316–328.
66 M. Friedrich, D. Teschner, A. Knop-Gericke and M. Armbrüster, Influence of Bulk Composition of the Intermetallic Compound ZnPd on Surface Composition and Methanol Steam Reforming Properties, *J. Catal.*, 2012, **285**(1), 41–47.
67 G. Deroubaix and P. Marcus, X-Ray Photoelectron Spectroscopy Analysis of Copper and Zinc Oxides and Sulphides, *Surf. Interface Anal.*, 1992, **18**(1), 39–46.
68 T. V. W. A. Janssens, New Approach to the Modeling of Deactivation in the Conversion of Methanol on Zeolite Catalysts, *J. Catal.*, 2009, **264**(2), 130–137.
69 S. Müller, Y. Liu, M. Vishnuvarthan, X. Sun, A. C. van Veen, G. L. Haller, M. Sanchez-Sanchez and J. A. Lercher, Coke Formation and Deactivation Pathways on H-ZSM-5 in the Conversion of Methanol to Olefins, *J. Catal.*, 2015, **325**, 48–59.
70 I. Yarulina, A. D. Chowdhury, F. Meirer, B. M. Weckhuysen and J. Gascon, Recent Trends and Fundamental Insights in the Methanol-to-Hydrocarbons Process, *Nat. Catal.*, 2018, **1**(6), 398–411.